# Interpretation of core ion cyclotron emission driven by sub-Alfvénic beam-injected ions via magnetoacoustic cyclotron instability

R. Ochoukov[1], K.G. McClements[2], R. Bilato[1], V. Bobkov[1], B. Chapman[3], S.C. Chapman[3], R.O. Dendy[2,3], M. Dreval[4], H. Faugel[1], J-M. Noterdaeme[1,5], M. Salewski[6], M. Weiland[1], ASDEX Upgrade Team[a)], and EUROfusion MST1 Team[b)]

[1]Max Planck Institute for Plasma Physics, Boltzmannstr. 2, D-85748 Garching, Germany
[2]Culham Centre for Fusion Energy, Culham Science Centre, Abingdon, Oxfordshire, OX14 3DB, UK
[3]Centre for Fusion, Space and Astrophysics, University of Warwick, Coventry, CV4 7AL, United Kingdom
[4]Institute of Plasma Physics, National Science Center 'Kharkov Institute of Physics and Technology', Kharkov, Ukraine
[5]Applied Physics Department, UGent, 9000 Gent, Belgium
[6]Technical University of Denmark, Department of Physics, DK-2800 Kgs. Lyngby, Denmark

a) see the author list in A. Kallenbach et al., Nucl. Fusion 57, 102015 (2017).
b) see the author list in H. Meyer et al., Nucl. Fusion 57, 102014 (2017).

## Abstract

Core ion cyclotron emission (ICE) signals have recently been observed in beam-heated plasmas on several tokamaks. In this manuscript we present experimental evidence in support of core ICE being generated by the magnetoacoustic cyclotron instability (MCI), itself driven by the velocity-space inversion of sub-Alfvénic beam-injected ions. The observed core ICE amplitude evolution in beam-heated plasmas is consistent with the MCI and is a result of competition between the beam ion fraction build-up (which increases the instability growth rate) and the slowing down of the dominant beam ion velocity component (which stabilizes the MCI). The oblique propagation angle is constrained to lie in the range 75-78$^o$, where the lower bound is governed by the fast wave reabsorption losses on plasma electrons and bulk ions and the upper bound is governed by the experimentally observed ICE amplitude growth time. Although the oblique MCI is a local theory and does not provide information on the radial mode localization, the calculated instability growth rates are broadly consistent with the observed dynamics of the core ICE amplitude on the ASDEX Upgrade tokamak.

## 1. Introduction

The velocity-space stability of fast ions (either wave-accelerated, beam-injected, or fusion-born) in D-T burning plasmas is crucial to the success of nuclear fusion as an energy source. If the fast ion distribution f becomes inverted in velocity space v (i.e. $\partial f/\partial v > 0$), free energy is available to drive instabilities in homogeneous plasmas [1, 2], which, in turn, may redistribute fast ions from their optimal state. One such instability-driven effect is thought to cause the ion cyclotron emission (ICE), and recent measurements show that it can exist in the plasma core near the magnetic axis [3-5]. In this manuscript we present experimental evidence supporting that core ICE is generated by the magnetoacoustic cyclotron instability (MCI) driven by the velocity-space inversion of sub-Alfvénic beam-injected ions. The MCI provides a viable explanation for the observed core ICE amplitude dynamics in beam-heated plasmas on ASDEX Upgrade: 1) the initial ICE amplitude growth follows the growth of the beam-injected fast ion

fraction (which increases the MCI growth rate); and 2) when the beam power is switched off, we observe a rapid ICE amplitude reduction (on the timescale much faster than the beam ion thermalization time), which matches the MCI growth rate reduction due to the slowing down of the dominant beam ion velocity component (which stabilizes the MCI).

## 2. Diagnostic and Experimental Setup Description

ICE signals in this study are generated via 21 deuterium NBI pulses (Fig. 1). Only one NBI source is used, with a beam incidence angle value that is intermediate between purely tangential and purely radial to the magnetic axis (Fig. 1 (a)). Each NBI pulse is 15 ms in duration ($P_{NBI}$ = 2.5 MW) and spaced apart by 300 ms (Fig. 1 (d)). The 300 ms duration is longer than the energy slowing down time $\tau_{SD}$ of the full-energy component of beam deuterium $D^+$ ions (birth energy $E_o$ = 92.5 keV, birth speed $v_o = 3.0\times10^6$ m $s^{-1}$). As a result, the fast deuterium ions do not accumulate/pile-up with each consecutive NBI pulse (Fig. 1 (g)). The fast deuterium ion contents for this discharge are obtained using TRANSP [6] and its fast ion NUBEAM module [7]. Note that each NBI pulse is preceded by a short (3 ms in duration), full power (2.5 MW) preconditioning pulse to decrease the rise time of the main NBI pulse. The ion cyclotron emission signals are quantified using a low-field side B-dot probe (Fig. 1 (a)). The signal from the B-dot probe is split into two halves via a 3dB splitter: one half of the signal is bandpassed (10-50 MHz) and rectified to extract the ICE amplitude; the second half is directly sampled at 125 MHz to obtain the ICE frequency spectra. The reader is referred to [3] for a full description of the ASDEX Upgrade ICE diagnostic used for this study. The plasma discharge is in L-mode to avoid edge localized modes and their influence on the probe measurements [8]. It is heated with ECRH power to prolong the discharge duration to 8 s (Fig. 1 (d)) and is in the upper single null configuration to prevent the H-mode transition. The on-axis magnetic field $B_T$ is –2.5 T (Fig. 1 (b)) and the plasma current value has two plateaux ($I_P$ = 0.465 MA and $I_P$ = 0.623 MA) (Fig. 1 (c)). The first 9 NBI pulses occur during the lower $I_P$ value, the last 11 NBI pulses take place during the higher $I_P$ value, and NBI pulse #10 takes place during the $I_P$ transition at $I_P$ = 0.55 MA (Fig. 1 (c)). The overall combination of the magnetic field (Fig. 1 (b)) and the core plasma density (Fig. 1 (e)) results in the Alfvén speed $c_A = 8.9\times10^6$ m $s^{-1}$, making the beam-injected ions sub-Alfvénic. 20 out of 21 NBI pulses generate ICE; no ICE signal is detected only during the 3rd NBI pulse (Fig. 2). Additionally, no detectable ICE signal is observed during any of the preconditioning pulses.

## 3. Experimental Results

The observed ICE frequencies (37-38 MHz) match the ion cyclotron frequency of the fundamental hydrogen cyclotron harmonic $\Omega_{H+}$ in the plasma center (Figs. 2 (a) and (c)), but also the 2nd harmonic deuterium $2\times\Omega_{D+}$. Both fast ion species are present in D-D plasmas heated with deuterium NBI: fast protons are generated via D-D nuclear fusion reactions and fast deuterons are injected by NBI. The fast ion birth speed favors the (super-Alfvénic) fusion proton over the (sub-Alfvénic) beam deuteron as the ICE driver [9]. However, the core ICE observation in hydrogen plasmas heated with hydrogen NBI (Fig. 3) strongly suggests the beam origin of this instability, as no other source of fast ions is present in these hydrogen discharges. The expected second harmonic hydrogen frequency is 76 MHz (core $B_T$ = –2.5 T), which appears in our ICE measurement at its aliased frequency 49 MHz = 125 MHz – 76 MHz (Fig.

3). No signal that would correspond to the fundamental hydrogen cyclotron harmonic in the core (~38 MHz) is observed, matching the deuterium results [3].

All 20 of the observed ICE bursts have a common feature: they all disappear within ~1 ms after the NBI turn-off time, much faster than the thermalization times of the beam ions (Fig. 2 (b)). The abrupt end to core ICE after the NBI turn-off time is not unique to ASDEX Upgrade plasmas: similar observations have been reported in the TUMAN-3M tokamak [5]. To quantify and follow the beam-injected deuteron population in the plasma on a short (~1 ms) timescale, we use TRANSP [6] and its NUBEAM module [7]. The time evolution of the beam-injected fast ion fraction during a single NBI pulse (#11) and the corresponding beam-injected ion velocity-space distribution are shown in Fig. 4. We use this data to estimate the instability growth rate in the following section.

## 4. Theoretical Modeling and Discussion

ICE is normally attributed to fast Alfvén wave excitation via the MCI, first discussed by Belikov and Kolesnichenko for the case of wave propagation strictly perpendicular to the magnetic field [10]. The analytical theory of the MCI was later extended by Dendy and co-workers to the case of oblique propagation [11]. An important feature of the obliquely-propagating MCI is that it can account for the excitation of ICE by sub-Alfvénic fast ions: this has been demonstrated analytically for ICE driven by charged fusion products in the Tokamak Fusion Test Reactor (TFTR) [12], and numerically for emission driven by beam ions in the Large Helical Device (LHD) [13]. As in most other conventional tokamaks, beam-injected fast ions in ASDEX Upgrade are born in the plasma at sub-Alfvénic velocities, and therefore it is worth exploring the possibility that the obliquely-propagating form of the MCI can account for the ICE discussed in the present paper.

Following [11] and [12], we assume that the beam ion distribution can be approximated as a shifted Gaussian in parallel velocity $v_{\parallel}$ and a delta function in perpendicular velocity $v_{\perp}$ [14]:

$$f = \frac{n_b}{2\pi^{3/2} u_{\perp} v_r} \exp\left(-\frac{(v_{\parallel} - u_{\parallel})^2}{v_r^2}\right) \delta(v_{\perp} - u_{\perp}). \quad (1)$$

Neglecting damping due to electrons and bulk ions, and assuming that the beam ion density $n_b$ is much smaller than the bulk ion density $n_i$ (consistent with our plasmas, see Fig. 4 (a)) it has been shown [12] that the growth ($\gamma > 0$) or damping ($\gamma < 0$) rate of the obliquely-propagating MCI for the $l$-th beam ion cyclotron harmonic (where the fast ion and the bulk plasma ion are of the same species) is given by (2)

$$\gamma = \frac{n_b}{n_i} \frac{\Omega_i^4}{[\Omega_i + (\omega - \Omega_i)N_{\parallel}^2][\Omega_i - (\omega + \Omega_i)N_{\parallel}^2]} \left(\frac{l\Omega_i}{k_{\parallel} v_r} \boldsymbol{M}_l - \frac{2u_{\perp}^2}{v_r^2} \eta_l \boldsymbol{N}_l\right) \frac{\sqrt{\pi}}{2\omega} e^{-\eta_l^2},$$

where $\Omega_i$ is the ion cyclotron frequency, $\omega$ is the mode frequency, $N_{\parallel}$ is the parallel refractive index of the wave defined with respect to the Alfvén speed, i.e. $N_{\parallel} = k_{\parallel} c_A/\omega$, where $k_{\parallel}$ is the parallel wavenumber, $\eta_l = (\omega - k_{\parallel} u_{\parallel} - l\Omega_i)/ k_{\parallel} v_r$ and the quantities $\boldsymbol{M}_l$ and $\boldsymbol{N}_l$ are defined by the expressions

(3)

(4)

$$\boldsymbol{M}_l = 2l\frac{\omega}{\Omega_i}\left(J_l'^2 + \frac{1}{z_b^2}(l^2 - z_b^2)J_l^2\right) - 2\frac{\omega^2 - \Omega_i^2}{\Omega_i^2}\frac{J_l J_l'}{z_b}\left[l^2 N_\perp^2 - (z_b^2 - 2l^2)N_\parallel^2\right] + \frac{2J_l J_l'}{z_b}(z_b^2 - 2l^2),$$

$$\boldsymbol{N}_l = -2l\frac{\omega}{\Omega_i}\frac{J_l J_l'}{z_b} + \frac{\omega^2 - \Omega_i^2}{\Omega_i^2}\left[N_\perp^2\frac{l^2 J_l^2}{z_b^2} + N_\parallel^2\left(\frac{l^2 J_l^2}{z_b^2} + J_l'^2\right)\right] + \frac{l^2 J_l^2}{z_b^2} + J_l'^2.$$

Here, $J_l$ denotes the Bessel function of order $l$ with argument $z_b = k_\perp u_\perp/\Omega_I$ and $N_\perp$ is the perpendicular refractive index of the wave ($N_\perp = k_\perp c_A/\omega$ where $k_\perp$ is the perpendicular wavenumber). As discussed in [12], $\boldsymbol{M}_l$ is generally negative in the sub-Alfvénic regime $u_\perp < c_A$ (applicable to beam ions in ASDEX Upgrade), while $\boldsymbol{N}_l$ is generally positive. It follows from this that the $\boldsymbol{M}_l$ term Eq. (2) is stabilizing while the $\boldsymbol{N}_l$ term is destabilizing if $\eta_l < 0$, which means that the Doppler-shifted mode frequency $\omega' \equiv \omega - k_\parallel u_\parallel$ lies below the cyclotron harmonic $l\Omega_i$ (the above expressions are applicable only for $k_\parallel > 0$ and must be modified for negative parallel wavenumbers [12]).

Specializing to the experimentally-relevant case of $l = 2$, we follow the time evolution of the beam-injected distribution (Fig. 5 (a)) calculated with TRANSP/NUBEAM and the corresponding instability growth rate (Fig. 5 (b)). In our calculations of the growth rate (Eq. (2)), we use the beam velocity spread $v_r/u_\perp = 0.08$ (consistent with Fig. 5 (a)) and the pitch = 0.5 (Fig. 4 (c)). Note that the $k_\parallel$ value is not measured in this experiment: to illustrate the trend expected from oblique propagation, we choose a nearly perpendicular propagation angle $\theta = 78^o$ (which provides us with $k_\parallel \approx (\omega/c_A)\cos\theta$). The fast ion fraction $n_b/n_i$ is given in Fig. 4 (a). The maximum growth rate first experiences an almost linear increase in value (Fig. 6), as the fast ion fraction in the core builds up during the NBI-on phase (Fig. 4 (a)). After the NBI source switches off, we observe a rapid drop of the maximum growth rate, which tracks the drop of the ICE signal (Fig. 6). Such behavior is in agreement with an observed correlation between edge ICE intensity and linear MCI growth rate for the case of sub-Alfvénic fusion-born $^3$He in TFTR plasmas (see. Fig. 6 in [12]). A correlation of this type has also been seen in fully nonlinear (particle-in-cell) simulations of fusion product-driven ICE in JET [15]. In our specific case, this rapid growth rate reduction and stabilization is attributed to the drop in the dominant beam speed value (and, hence, $u_\perp$), see Fig. 5 (a) for t = 4.669 s. In fact stabilization could occur even when the linear growth rate is positive, due to electron and bulk ion damping. The high sensitivity of $\gamma/\Omega_\alpha$ (where $\Omega_\alpha$ is the fast deuteron cyclotron frequency) to $u_\perp$ provides a possible explanation of the rapid disappearance of ICE following the end of the beam heating phase, since the presence of collisional friction in the absence of a beam source means that $u_\perp$ starts to drop immediately.

The importance of the dominant beam-injected fast ion velocity component (which determines $u_\parallel$ and $u_\perp$) is highlighted in Fig. 5. However, the propagation angle $\theta$ is another key parameter that governs the growth rate of the oblique MCI. The choice of $\theta = 78^o$ is not arbitrary, this angle corresponds to the calculated MCI growth rate value $\sim 3\times10^{-6}\ \Omega_\alpha = 360\ s^{-1}$ (Fig. 5 (b)) that matches the inverse of the experimentally measured ICE amplitude growth time $1/(2\times10^{-3}\ s) = 500\ s^{-1}$. As the propagation angle approaches $90^o$, the growth rate value rapidly diminishes (Fig. 7), and the growth rate becomes stabilizing at the strictly perpendicular angle. While the MCI theory helps us quantify what happens to the ICE amplitude at the place of its origin, it is equally important to determine if the resulting fast wave excitation has the necessary properties

to reach the plasma periphery (where the probes are located) without being reabsorbed by the bulk plasma. To perform this estimate we set runs of FELICE code [16] in such a way that the MCI waves are excited with a short one-strap antenna whose location is changed from the usual edge position to the plasma core. Realistic radial plasma density, electron temperature, and magnetic field profiles are used to calculate how much of the fast wave power is lost to the electrons and to the ions as a function of the parallel wave number (Fig. 8). These approximate results reveal that only fast waves with low $k_{\|}$ are capable of reaching the plasma boundary and, in principle, be detected by the probes without suffering a significant power loss to the plasma electrons. The low $k_{\|}$ values are consistent with the MCI picture presented earlier that constrains the $k_{\|}$ value to a small but non-zero value in order for the instability to develop. As an example, the fast wave losses to the plasma electrons and bulk ions remain below 50% for $k_{\|} < 7$ m$^{-1}$ (Fig. 8). Using the experimental values for $\omega = (2\pi)\times 40\times 10^6$ s$^{-1}$ and $c_A = 9\times 10^6$ m s$^{-1}$ we obtain $\theta > 75^o$ from $k_{\|} \approx (\omega/c_A)\cos\theta$, in line with $\theta = 78^o$ that we use for our growth rate calculations. Note that the ASDEX Upgrade ICE diagnostic can, in principle, measure the parallel wavenumber. However, the presence of "frequency splitting" (Fig. 2 (a)) complicates mode identification due to the appearance of beat waves that continuously scan the signal phase between two nearby probes (see, for example, Fig. 5 in [3]). The origin of spectral splitting is unknown but the phenomenon is observed on other tokamaks [4, 5]. It is clear that further theoretical and experimental studies are needed to fully explain the phenomenon of core ICE.

Although the digitization rate (125 MHz) of the ASDEX Upgrade ICE diagnostic limits the observed harmonic number $l$ in the analyzed discharge to $\leq 2$, other tokamaks report core ICE signals for $l > 2$ [4, 5]. We also reported previously the observation of the 2$^{nd}$, 3$^{rd}$, and 4$^{th}$ deuteron cyclotron harmonics in a discharge at low $B_T = -1.8$ T [3]. The ICE spectral peaks are narrow and their frequencies are observed to correspond to harmonics of the ion gyrofrequency near the magnetic axis. This implies that the excitation must be strongly localized to a region of the vertical surface of constant magnetic field strength that passes through the magnetic axis. On that surface, the most likely locus is at the core of the plasma, where the potential for creating a population inversion in the velocity distribution of NBI ions is greatest: owing, as discussed, to local competition between fueling and slowing-down. Given such a population inversion, excitation of ICE through the MCI can follow, again as discussed.

Finally, we would like to mention that the presented oblique MCI theory does not provide us with an estimate of the mode radial position in the plasma, making it a local theory. Theoretical works of Coppi et al. [17] and Gorelenkov et al. [18] do account for the global mode structure. However, their particular choice of the potential function $V(r)$ ($\sim r^{-2}$, where r is the minor radius) that governs the radial position of the mode, diverges at the plasma center and, hence, cannot account for the observed core ICE.

## 5. Summary

To summarize, we present experimental evidence in support of core ICE being generated by the obliquely propagating MCI driven by the velocity-space inversion of (sub-Alfvénic) beam-injected fast ions. The observed core ICE amplitude growth is a result of competition between the fast ion fraction build-up (which increases the MCI growth rate) and the slowing down of the dominant beam ion velocity component (which stabilizes the MCI). The propagation angle is constrained to lie in the range 75-78$^o$, where the lower bound is governed by the fast wave reabsorption losses on plasma electrons and bulk ions and the upper bound is governed by the experimentally observed ICE amplitude growth time. Although the oblique MCI is a local

theory and does not provide information on the mode radial localization, the calculated instability growth rates are broadly consistent with the observed dynamics of the core ICE amplitude on the ASDEX Upgrade tokamak. The commonly-observed "frequency splitting" remains unexplained by the MCI theory. It is clear that further theoretical and experimental studies are needed to fully describe the phenomenon of core ICE.

## 6. Acknowledgements

This work has been carried out within the framework of the EUROfusion Consortium and has received funding from the Euratom research and training programme 2014-2018 and 2019-2020 under grant agreement No 633053. The views and opinions expressed herein do not necessarily reflect those of the European Commission. The contribution of Rodolphe D'Inca to the development of the ICE diagnostic on ASDEX Upgrade is gratefully acknowledged.

## References

[1] Kolesnichenko, Ya. I., Sov. J. Plasma Phys. 6 (5), Sept.-Oct. 1980, p. 531-532.
[2] J.G. Cordey, R.J. Goldston, D.R. Mikkelsen, Nucl. Fusion, Vol. 21, No. 5 (1981).
[3] R. Ochoukov, V. Bobkov, B. Chapman, R. Dendy, et al., Rev. Sci. Instrum. 89, 10J101 (2018).
[4] K. E. Thome, D. C. Pace, R. I. Pinsker, O. Meneghini, C. A. del Castillo, and Y. Zhu, Rev. Sci. Instrum. 89, 10I102 (2018).
[5] L. G. Askinazi, A. Belokurov, D. B. Gin, V. A. Kornev, S. V. Lebedev, A. E. Shevelev, A. S. Tukachinsky and N. A. Zhubr, Nucl. Fusion 58, 082003 (2018).
[6] https://transp.pppl.gov (Version 18.2) DOI: 10.11578/dc.20180627.4.
[7] A. Pankin, D. McCune, R. Andre, G. Bateman, A. Kritz, "The Tokamak Monte Carlo Fast Ion Module NUBEAM in the National Transport Code Collaboration Library", Computer Physics Communications Vol. 159, No. 3 (2004) 157-184.
[8] R. Ochoukov, V. Bobkov, H. Faugel, H. Fünfgelder, J. Jacquot, J.-M. Noterdaeme, G. Suárez López, and ASDEX Upgrade Team, Rev. Sci. Instrum. 87, 11D301 (2016).
[9] R. O. Dendy, C. N. Lashmore-Davies, and K. F. Kam, Phys. Fluids B 4 (12), December 1992.
[10] Belikov V.S. and Kolesnichenko Ya.I. 1975 *Zh. Tekh. Fiz.* **45** 1798; 1976 *Sov. Phys. Tech. Phys.* **20** 1146.
[11] Dendy R.O., Lashmore-Davies C.N., McClements K.G. and Cottrell G.A. 1994 Phys. Plasmas 1, 1918.
[12] McClements K.G., Dendy R.O., Lashmore-Davies C.N., Cottrell G.A., Cauffman S. and Majeski R. 1996 Phys. Plasmas 3, 543.
[13] Reman B.C.G., Dendy R.O., Akiyama T., Chapman S.C., Cook J.W.S, Igami H., Inagaki S., Saito K. and Yun G.S. 2016 Proc. 43rd EPS Conf. Plasma Phys., Leuven, Belgium July 4-8 2016, P2.041. http://ocs.ciemat.es/EPS2016PAP/pdf/P2.041.pdf
[14] D. Moseev and M. Salewski, Physics of Plasmas 26, 020901 (2019).
[15] Cook J.W.S., Dendy R.O. and Chapman S.C. 2013 Plasma Phys. Control. Fusion 55, 065003.
[16] M. Brambilla, Plasma Physics and Controlled Fusion, Vol. 31, No. 5. pp, 123 to 151, 1989.
[17] B. Coppi, S. Cowley, R. Kulsrud, P. Detragiache, and F. Pegoraro, Physics of Fluids 29, 4060 (1986).

[18] N. N. Gorelenkov and C. Z. Cheng, Physics of Plasmas 2, 1961 (1995).

## Figures

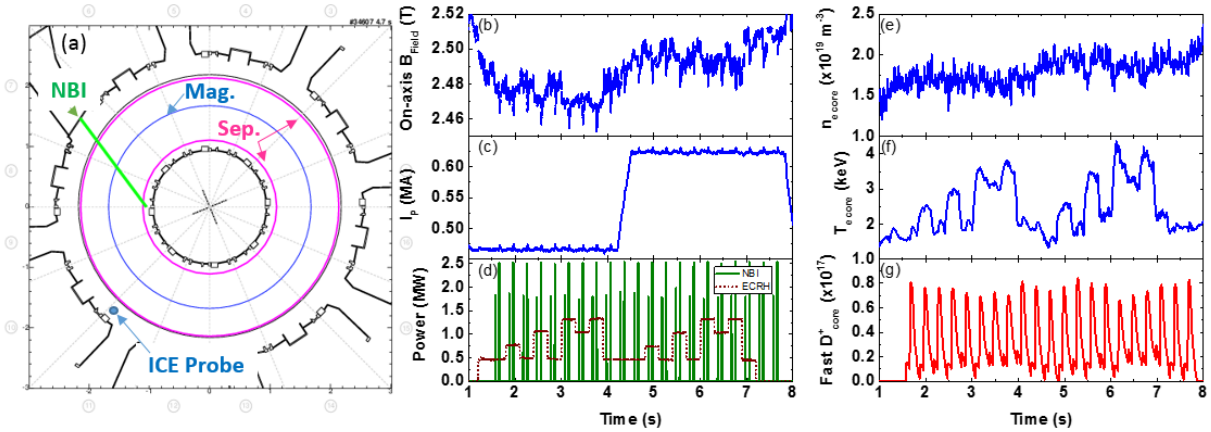


FIG 1. (a) The top cross-sectional view of ASDEX Upgrade. The magnetic axis (Mag.), the separatrix (Sep.), the ion cyclotron emission (ICE) probe, and the neutral beam injection (NBI) geometry (Source #8) are shown. Key discharge parameters for discharge #34607 are shown: (b) the on-axis magnetic field $B_{Field}$, (c) the plasma current $I_P$, (d) the NBI and the electron cyclotron resonance (ECRH) heating powers, (e) the core plasma density $n_{e\ core}$, (f) the core electron temperature $T_{e\ core}$, and (g) the core fast deuterium $D^+$ content.

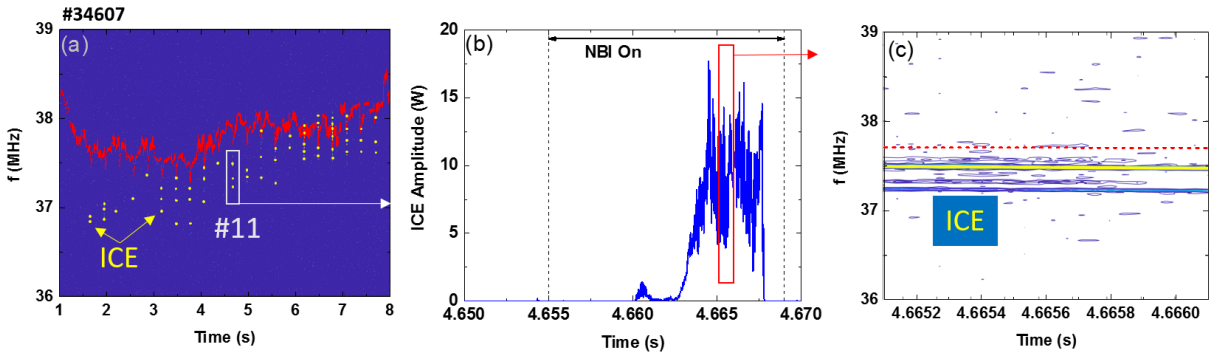


FIG. 2. (a) Ion cyclotron emission (ICE) spectra during all 21 deuterium NBI pulses; (b) an example of a detailed ICE amplitude time history during a single NBI pulse, the time when the NBI power remains on is shown; (c) a detailed time history of ICE spectra during NBI pulse. The red dotted line in (a) and (c) shows the on-axis value of the second harmonic deuterium cyclotron frequency, as estimated from magnetic equilibrium reconstruction.

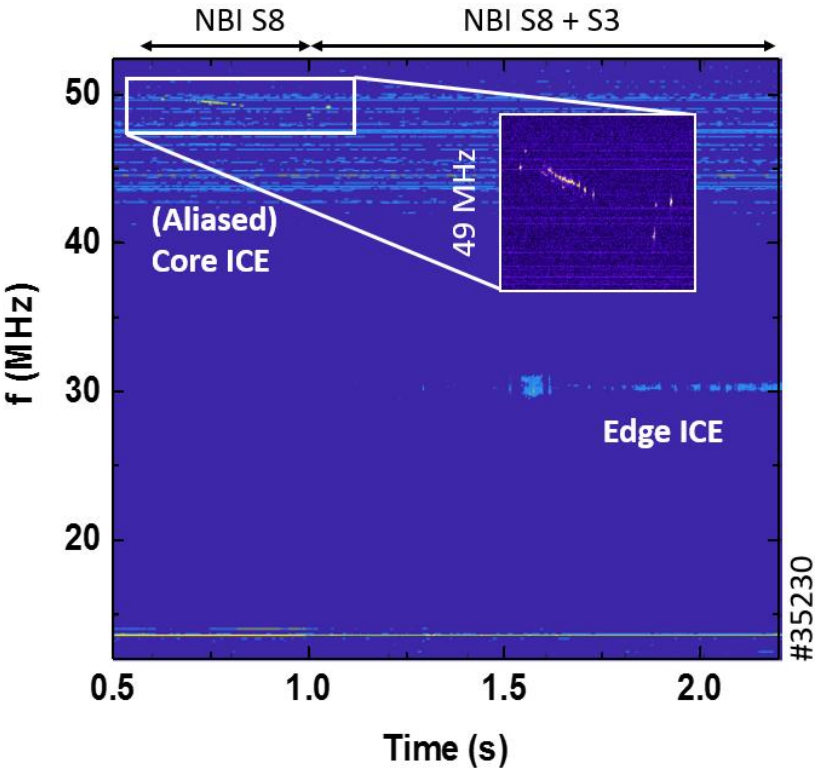


FIG. 3. Observation of core ICE in hydrogen plasma heated by hydrogen NBI (Source #8 shown in Fig. 1 (a)). The signal appears at its aliased frequency 49 MHz = digitization frequency125 MHz – actual 76 MHz.

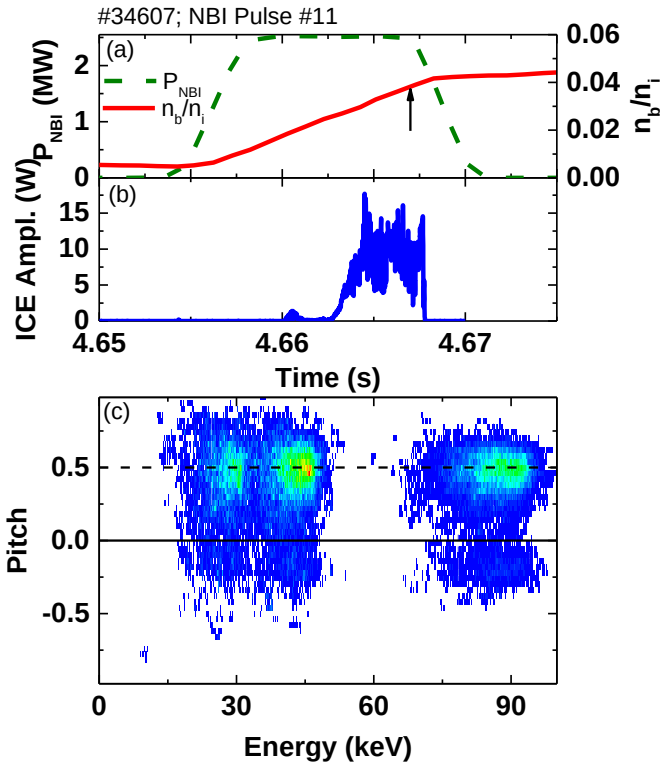


FIG. 4. A detailed time evolution of (a) the NBI power $P_{NBI}$ and the beam ion fraction $n_b/n_i$ and (b) the ICE amplitude during NBI pulse #11. The vertical arrow in (a) indicates the time at which the fast ion distribution function (in pitch-energy space) is computed via TRANSP/NUBEAM, shown in (c). A dashed horizontal line in (c) corresponds to the dominant pitch value = 0.5. The three peaks in (c) correspond to the full, the ½, and the 1/3 energy components of the beam-injected ions.

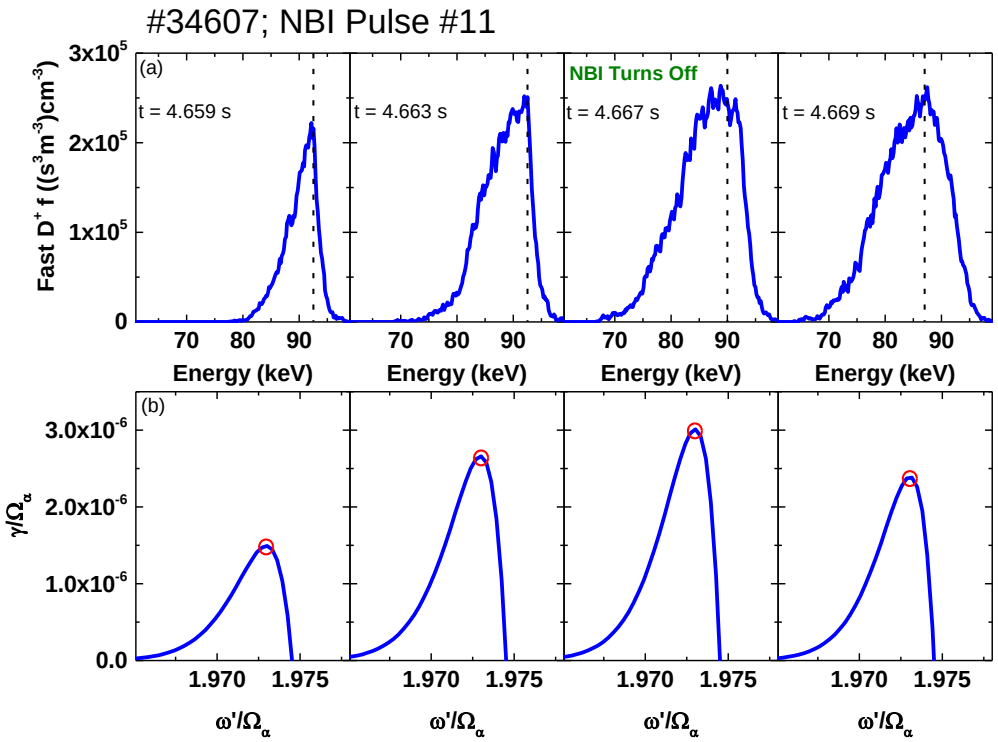


FIG: 5. Time evolution of (a) TRANSP-calculated beam ion velocity distribution and (b) the MCI growth rate from Eq. (2) for an example NBI pulse (#11), $\omega' \equiv \omega - k_{\parallel}u_{\parallel}$. The vertical dashed lines in (a) show the dominant beam energy and the red circles in (b) show the maximum growth rate values. The NBI turn off time is indicated in (a). The propagation angle $\theta = 78^{o}$.

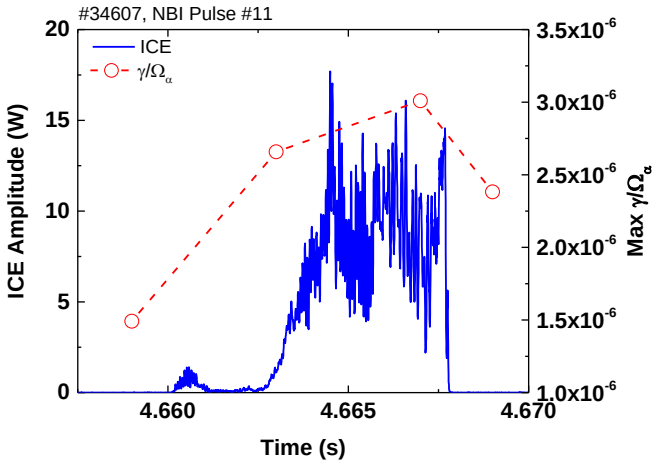


FIG: 6. The time evolution of the ICE amplitude and the maximum instability growth rate $\gamma/\Omega_\alpha$, as computed via Eq. (2) for the case of $l = 2$. The maximum growth rate values are taken from Fig. 5 (b).

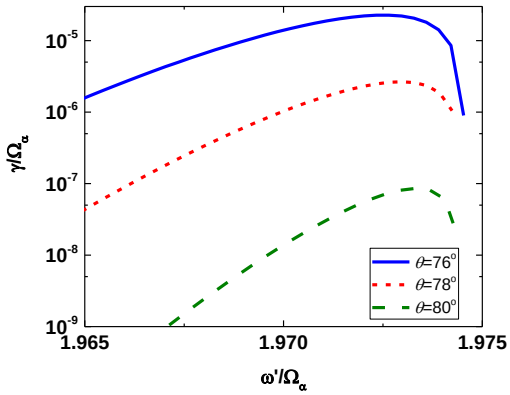


FIG. 7. Oblique MCI growth rate values for three different propagation angles: long dashed green line $\theta = 80^{o}$; short dashed red line $\theta = 78^{o}$ and solid blue line $\theta = 76^{o}$.

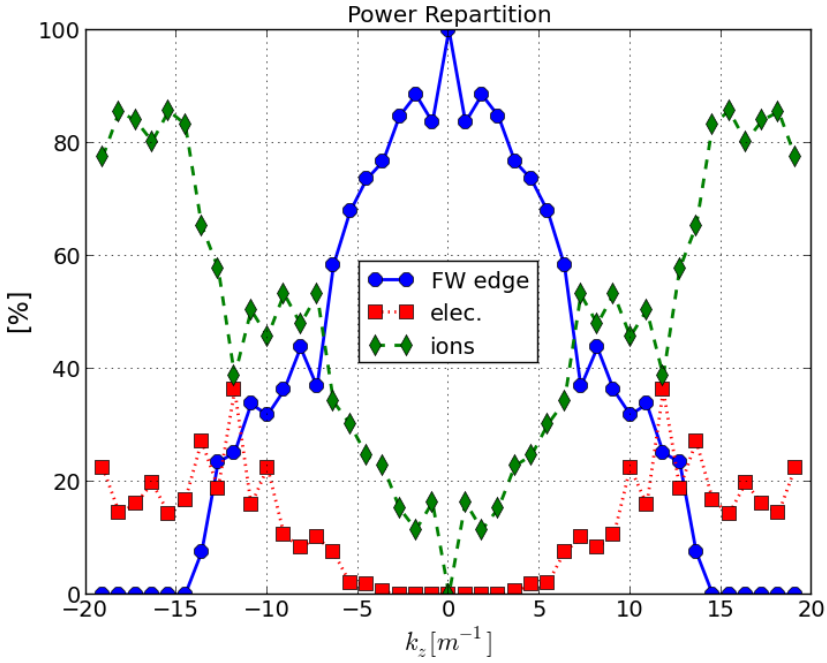


FIG. 8: The fast wave (FW) power repartition as a function of the parallel wave number $k_z$, as estimated by FELICE [16]. The FW edge (blue circles) refers to the fast wave power that reaches the plasma boundary without being reabsorbed on either the plasma electrons (red squares) or the bulk ions (green diamonds).